Effect of electrostatic interactions on the dynamics of semiflexible monodisperse DNA fragments

ARTICLE *in* THE JOURNAL OF CHEMICAL PHYSICS · OCTOBER 2000

Impact Factor: 2.95 · DOI: 10.1063/1.1290477

Effect of electrostatic interactions on the dynamics of semiflexible monodisperse DNA fragments

Hui Liu[a)]
Department of Chemistry, Stanford University, Stanford, California 94305-5080

Jacek Gapinski and Lidia Skibinska
Institute of Physics, Adam Mickiewicz University, Umultowska 85, 61-614 Poznan, Poland

Adam Patkowski
Institute of Physics, Adam Mickiewicz University, Umultowska 85, 61-614 Poznan, Poland
and Max Planck Institute for Polymer Research, Ackermannweg 10, 55128 Mainz, Germany

R. Pecora[b)]
Department of Chemistry, Stanford University, Stanford, California 94305-5080

(Received 1 May 2000; accepted 12 July 2000)

The dynamics of three monodisperse linear duplex DNA fragments—a 2311 base pair restriction fragment and 1500 and 1100 base pair polymerase chain reaction fragments—in dilute solution are studied as functions of added salt (NaCl) concentration by dynamic light scattering-photon correlation spectroscopy. Translational diffusion coefficients and intramolecular relaxation times are extracted from the measured light scattering intensity time autocorrelation functions as the added salt concentration is reduced from 100 mM to approximately 0.1 mM. The relaxation times of the first intramolecular mode increase as the added salt concentration is lowered. The dependence of the translational diffusion coefficient D on the added salt concentration is not very large, although it exhibits a maximum for all three fragments. The maximum is interpreted as the consequence of two opposing effects—the stiffening of the molecule that produces an increase of the size (decrease of D) as the added salt concentration is lowered, and the coupling of the diffusion of the DNA through the electrostatic forces to the motion of the small and other polyions in the solution that results in an increase of its mobility (increase of D). The increase of the slowest intramolecular relaxation times as the salt concentration is lowered is interpreted in terms of a theory relating this time to the mean-squared radius of gyration of the molecule.
[S0021-9606(00)50638-2]

I. INTRODUCTION

We have in previous publications examined in detail the dynamics of a 20 base pair duplex oligonucleotide using dynamic light scattering photon correlation spectroscopy, depolarized Fabry–Perot interferometry and small angle x-ray scattering.[1,2] The oligonucleotide is a high charge density, rigid polyion. Molecular flexibility adds further complexity to the solution dynamics of longer DNAs. Theories of the solution dynamics of flexible and semiflexible macromolecules in dilute solution have been developed for molecular stiffness ranging from rigid rod to Gaussian coil. Despite the large number of experimental studies that have focused on flexible polymer solution dynamics in the past several decades, the contributions of electrostatic interactions are often neglected due to the lack of adequate theoretical treatments and the lack of good model semiflexible polyelectrolytes. In this study, we used well defined, monodisperse, 1100, 1500, and 2311 base pair linear duplex DNA fragments as model systems to study the contributions of electrostatic interactions and molecular flexibility to the solution dynamics.

Plasmid pLH2311 bp is one of a set of DNA fragments previously constructed by Lewis *et al.*[3] Its superhelical form was studied by Seils and Pecora in dilute and semidilute solutions using dynamic light scattering (DLS).[4] Seils and Pecora[5] and Tracy, Newman, and Pecora[6] have performed DLS studies on its relaxed circular form at various salt concentrations. Sorlie and Pecora[7,8] have previously done DLS experiments on the linear form as well as on shorter restriction fragments 1010, 762, and 367 bp in length in 100 mM NaCl, 10 mM Tris, and 1 mM EDTA buffer solutions at $p\mathrm{H}=8$. Sorlie and Pecora compared the predictions of various theories for the diffusion coefficients of semiflexible macromolecules and theories of intramolecular relaxation of linear chains with their experimental DLS results on the solution dynamics of these four DNA restriction fragments. They did not, however, study polyelectrolyte effects.

The linear DNAs were previously studied at relatively high added salt concentration ($C_s=103$ mM, including the 3 mM sodium ion concentration from the buffer) conditions under which polyelectrolyte effects are thought to be relatively small. For these highly charged linear molecules, we expect the molecular stiffness (persistence length) to change

[a)]Present address: Materials and Process Laboratory, Seagate Technology, 311 Turquoise Street, Milpitas, California 95035. Electronic mail: Hui_Kathy_Liu@notes.seagate.com
[b)]Author to whom correspondence should be addressed.

with solution ionic strength.[9] In solutions containing a high concentration of added salt, the intramolecular electrostatic interaction is screened by small ions in solution, while in low salt solutions, the electrostatic repulsion between the same charged subunits on the DNA backbone enhances the molecular stiffness. Thus, the persistence length is expected to increase as the added salt concentration in the buffer solution decreases. This increase in the persistence length should give a decrease in the translational diffusion coefficient. However, the interactions of the polyion with the small ions and with each other increase as the salt concentration is lowered and tend to raise the diffusion coefficient. In this study we examine the dynamics of the linear form of the 2311 bp duplex DNA and two duplex polymerase chain reaction (PCR) fragments of length 1100 and 1500 bp in solutions with varying amounts of added salt (NaCl). We compare our experimental results with previous results on a series of DNAs at high added salt, with results at various salt concentrations on the relaxed circular form of the 2311 bp DNA,[5,6] and with predictions of theories incorporating the range of stiffness of the molecule, and, where available, include polyelectrolyte effects in the calculation.

II. EXPERIMENT

A. Sample preparation

The 2311 bp plasmid DNA was prepared as described by Lewis *et al.*[3,10] The plasmid DNA was digested by Pvu II enzyme at 37 °C for about 2 h in $p\mathrm{H}=7.5$ buffer containing 10 mM Tris-HCl, 50 mM NaCl, 10 mM $MgCl_2$, and 1 mM dithiothretol. A phenol/chloroform extraction was performed immediately after the Pvu II digestion. Three ether extractions were followed. The DNA was precipitated twice with ethanol and re-suspended in TE buffer which contains 10 mM Tris-HCl, 1 mM Na_2EDTA, and 1 mM NaOH, $p\mathrm{H}=8.0$. The DNA was checked for impurities with gel electrophoresis on a 1% agarose gel. A single band was observed and was compared with the superhelical 2311 base pair DNA and circular 2311 base pair DNA bands on the same gel. Gel electrophoresis was repeated throughout the DLS experiments. No degradation of the plasmid was observed. Different ionic strength solutions were prepared by filtering TE buffer containing concentrated NaCl through a 0.2 μm Anotop filter into a precleaned DNA solution. One molar NaCl was used to achieve the 7 mM ionic strength solution; 4 M NaCl was used for higher salt concentration solutions. After reaching equilibrium, the DNA solution in TE buffer with added salt was filtered through a 0.45 μm filter into another precleaned, dust free cuvette. The concentration of added salt was determined by weighing the sample before and after the addition of TE buffer containing concentrated NaCl. DNA concentrations were determined by UV absorbency at 260 nm at proper dilution.

The 1100 and 1500 bp PCR fragments were synthesized by Dr. Damian Labuda of the University of Montreal using standard PCR techniques. In the PCR method small amounts of a given DNA fragment are amplified in the standard enzymatic reaction of DNA replication. Starting the reaction requires short pieces (20–30 bp) of DNA complementary to the ends of the matrix DNA (primers) to be present. Purification of the resultant sample was performed using a standard purification kit (QIAquick, Qiagen GmbH, Germany). The samples were dialyzed on Centricon-100 concentrators (Amicon, MA, USA). In this procedure the solution of DNA is dialyzed by pressing the solvent through a membrane with small pores (100 kDa molecular weight cut-off). Several dialysis cycles were performed on each sample. The buffers used contained 10 mM Tris to maintain solution $p\mathrm{H}$ at 7.6, and various amounts of added NaCl to achieve different solution ionic strengths. All buffer solutions (except those denoted ''no added salt'') also contained 1 mM Na_2EDTA to chelate any trace amounts of multiply charged ions.

B. Dynamic light scattering: Photon correlation spectroscopy experiments

The photon autocorrelation functions were measured on the same dynamic light scattering set ups as described in previous publications[1,2] except that the 2311 bp fragment experiments used a Brookhaven BI2030AT digital correlator with 136 real time data points. The light sources were argon ion lasers operating at either 488.0 or 514.5 nm. The experiments on the 1500 and 1100 bp fragments used an ALV 5000 autocorrelator. The sample holder was immersed in index matching fluid to reduce reflection of light from the surface of sample cell walls. All experiments for this study were carried out at 20 °C. Laser powers between 0.2 and 0.9 W were used. Apparent scattering angles from samples in rectangular cuvettes were corrected using the refractive index of the solvent and refractive index of matching fluid. Scattering angles between 30° and 140° were used in the measurement of photon autocorrelation functions. Only those data with a difference between the calculated and measured baseline $\Delta B<0.1\%$ were considered, except for data measured at a scattering angle of 33°, where $\Delta B<0.2\%$ were accepted.

C. Data analysis

Photon autocorrelation functions were analyzed using CONTIN,[11–13] the constrained regularization method for a nonlinear least-squares fit to numerically find the inverse Laplace transform of the correlation functions. As pointed out in our earlier studies, CONTIN does not require knowledge of the number of exponentials (or decay rates) in the photon autocorrelation function. A full description of the use of CONTIN as applied to DLS from DNA solutions has been given previously.[7,8] In many cases, sums of exponentials were also used to fit the data. No significant discrepancies were obtained between the two data fitting methods.

III. RESULTS AND DISCUSSION

Photon autocorrelation functions for 83–107 μg/ml solutions of the linear 2311 base pair DNA fragment in $p\mathrm{H}=8$ TE buffer of five different ionic strengths were measured at 20 °C and various scattering angles. Measurements of the 1100 and 1500 bp fragments were done at 250 and 200 μg/ml concentration and $p\mathrm{H}=7.6$ at several added salt con-

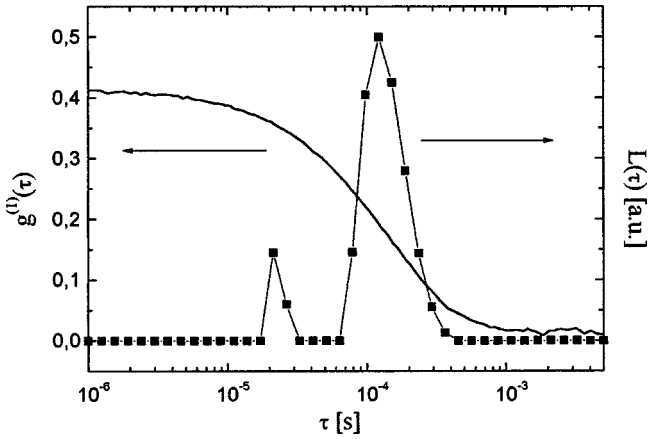

FIG. 1. A typical correlation function and corresponding relaxation time distribution for a 1100 bp DNA sample at 2 mM NaCl and DNA concentration=250 μg/ml.

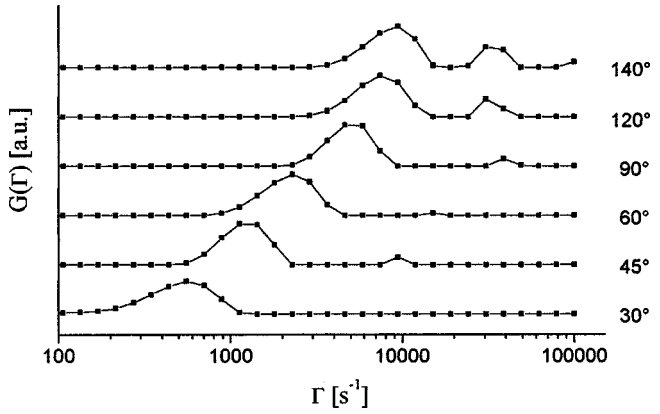

FIG. 2. Decay rate distribution obtained from CONTIN analysis of a correlation function measured at different scattering angles for the 1100 bp DNA at 2 mM NaCl.

centrations. The buffer was the same as for the 2311 except for the sample with ''no added salt'' (estimated to be 0.1 mM in salt).

Experimental intensity autocorrelation functions can be expressed as

$$C(t)=B+A|g^{(1)}(t)|^2, \tag{1}$$

where t is the delay time, B is the baseline, and A is an experimental constant dependent on the experimental optics. $g^{(1)}(t)$ is the first order normalized scattered electric field time autocorrelation function. Figure 1 shows a typical $g^{(1)}(t)$ measured for the 1100 bp DNA in 2 mM added NaCl and a scattering angle of 120° at 20 °C.

The normalized first order correlation function $g^{(1)}(t)$ can be characterized by a continuous distribution of relaxation rates

$$g^{(1)}(t)=\int_0^\infty G(\Gamma)\exp(-\Gamma t)d\Gamma, \tag{2}$$

where $G(\Gamma)$ is a normalized distribution function and Γ is the relaxation rate. Figure 1 also shows the normalized $G(\Gamma)$ as determined by CONTIN analysis of the first order correlation function shown in the same figure.

Figure 2 shows a set of decay rate distribution functions ($G(\Gamma)$) from CONTIN for the 1100 bp DNA sample at 2 mM added NaCl at different scattering angles. A faster peak contributes up to 10% to the correlation function. Notice that the decay rate at the maximum of the slower peak increases with increasing scattering angle (increasing scattering vector length). No evidence for ''slow modes'' was found in any of the correlation functions studied.[1,2,6] The relaxation rates Γ can be converted into diffusion coefficients D and into apparent hydrodynamic radii R_h using the Stokes–Einstein relation with stick boundary conditions,

$$\Gamma=Dq^2=\frac{kT}{6\pi\eta R_h}q^2. \tag{3}$$

Examples of the scattering vector length (q) angle dependencies of the apparent hydrodynamic radii for the 1100 and 2311 base pair DNAs are shown in Fig. 3.

A similar CONTIN analysis of $g^{(1)}(t)$ of the linear 2311 bp DNA shows that, as expected, autocorrelation functions measured at the low scattering angle 33° are from a single decay process. At higher scattering angles, however, multiple decay processes are observed and the slower peak becomes wider.

The same trend was observed for this DNA fragment[7] and for a 1010 base pair DNA fragment[8] by Sorlie and Pecora in 100 mM added salt solution. Observations by Sorlie and Pecora[8] on a series of DNA fragments with various lengths have shown that the apparent decrease of the hydrodynamic radius with increasing scattering angle is less profound as the DNA length decreases. When the DNA length decreases to 762 bp, a decrease of the apparent hydrodynamic radius is no longer observed.

Pecora[14–16] showed for small scattering angles and/or small molecules, that translational motion of the molecule under investigation is the sole source of an exponential decay in the intensity autocorrelation function of the scattered light. For larger scattering angles and large molecules, contributions from the intramolecular/rotational relaxation modes become important. The first order DLS autocorrelation function can be expressed as

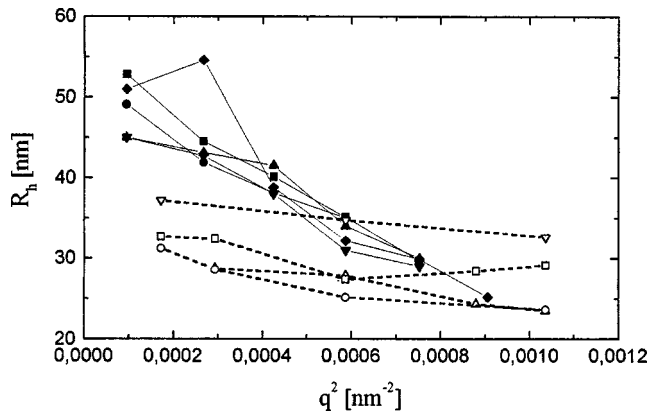

FIG. 3. Dependencies of the hydrodynamic radii of the 1100 (open symbols) and 2311 (filled symbols) base pair DNA on the scattering vector. The different curves for each DNA are for different added salt concentrations.

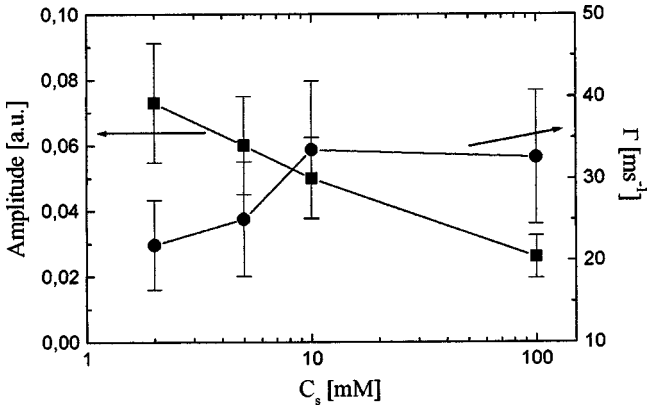

FIG. 4. Amplitude (■) and decay rate (●) of the intramolecular/rotational mode measured at the scattering angle of 140° for the 1100 bp DNA as a function of ionic strength.

$$g^{(1)}(t)=A_0\exp(-\Gamma_0 t)+A_1\exp(-\Gamma_1 t)+\cdots$$
$$=A_0\exp(-q^2Dt)+A_1\exp\left(-q^2Dt-\frac{t}{\tau_1}\right)+\cdots, \quad (4)$$

where A_0 gives the contribution of pure translational motion to the correlation function, and A_1 gives the contribution of the combined mode from both translational and intramolecular/rotational relaxation to the correlation function. For even larger scattering angles, additional terms make important contributions to the correlation function in Eq. (4).

Translational diffusion coefficients were calculated from the slowest, dominant peak of the CONTIN analysis of correlation functions measured at the lowest scattering angle, 33°. The intramolecular/rotational relaxation time τ_1 that can be extracted from the second decay frequency of the correlation functions, as indicated by Sorlie and Pecora,[8] is probably neither pure rotational motion nor pure internal breathing of the molecule. We call this relaxation time the ''intramolecular'' decay time. It would be related to the ''rotational relaxation time'' in the limit that the chain became very stiff. Figure 4 shows the amplitude and relaxation time for the intramolecular mode for the 1100 bp fragment as a function of added salt concentration. Notice that the error bars can be rather large for the relaxation time. The measured translational diffusion coefficients of the linear fragments at different ionic strengths measured at 20 °C are listed in column 3 of Table I and the intramolecular decay times τ_1

TABLE I. Experimental diffusion coefficients and derived quantities for the three DNA fragments.

1 C_s (mM)	2 κ^{-1} (nm)	3 D (10^{-8} cm^2/s)	4 $\langle R_G^2\rangle^{1/2}$ (nm) (OH)	5 P_{app} (nm)	6 P_{el} (nm)	7 P_T (nm)	8 $D_{(YF)}$ (10^{-8} cm^2/s)	9 $R_G(\tau)$ (nm)	10 ϵ_{el}
(a) 1100 Base pair DNA									
2	6.83	6.92±0.06	77.6	139	15.3	48.3	6.51	86	0.285
5	4.32	8±1	70.2	139	6.4	39.4	6.51	86	0.247
10	3.05	7.40±0.15	67.6	67	3.2	36.2	6.87	72	0.198
100	0.966	6.01±0.05	66.8	51	0.32	33.3	7.09	66	0.071
(b) 1500 Base pair DNA									
0.1	30.5	5.25±0.37	228	300	265	300	4.96	127	0.093
2	6.83	6.41±0.39	92.7	140	16	51	5.12	110	0.311
5	4.32	6.76±0.21	84.1	140	6.4	41.4	5.12	110	0.267
8	3.41	6.93±0.21	81.9	88	4.0	39	5.32	97	0.230
20	2.16	6.52±0.13	80	88	1.6	36.6	5.32	97	0.160
200	0.683	6.3±0.16	81.6	50	0.16	35.2	5.73	80	0.054
(c) 2311 Base pair DNA									
3	5.56	4.07±0.30	131	92	10.6	51.6	3.85	137	0.3016
7	3.63	4.37±0.12	121	74	4.6	45.6	3.98	121	0.2415
27	1.85	4.92±0.39	112	61	1.2	42.2	4.11	135	0.1381
63	1.21	4.76±0.07	109	56	0.51	41.5	4.17	131	0.0926
103	0.95	4.56±0.13	108	55	0.31	41.3	4.19	129	0.073
178	0.72	4.21±0.15	107	5	0.18	41.2	4.21	106	0.0558

Columns:
(1) Added salt concentration.
(2) The Debye–Huckel screening parameters, κ^{-1}, were calculated from the added salt only.
(3) Experimental values of the DNA translational diffusion coefficient D.
(4) The root-mean-square radii of gyration were calculated with P_T listed in column 7 and the Odijk–Houwaart equation, Eq. (5).
(5) Apparent persistence lengths were calculated with $\langle R_G^2\rangle^{1/2}$ listed in column 4 and the Benoit and Doty equation, Eq. (8).
(6) The electrostatic persistence lengths were calculated using the Odijk–Houwaart theory, Eqs. (6) and (7).
(7) The total persistence lengths (sum of electrostatic persistence length and intrinsic persistence length) were calculated based on the intrinsic persistence length $P=53.5$ nm which was obtained from the Yamakawa–Fujii theory and the measured translational diffusion coefficients of the DNAs at the highest salt concentration conditions.
(8) Diffusion coefficients from the Yamakawa–Fujii relation and the apparent persistence lengths in column 5 using an assumed DNA diameter=25 Å.
(9) The root-mean-square radii of gyration were calculated from the Seils–Pecora scaling law, Eq. (13), using experimental values of τ_{int} and D and taking as a reference R_G the value from high salt data.
(10) Excluded-volume parameters were calculated using Eq. (9).

TABLE II. Intramolecular relaxation times and theoretical comparison.

1 C_s (mM)	2 C_{DNA}/C^*	3 τ_{int} (μs)	4 τ_{YY} (μs)	5 $\tau^{RZ}_{free\text{-}dra}$ (μs)	6 τ^{RZ}_{nondra} (μs)
(a) 1100 Base pair DNA					
2	1.3	41±12	327	125	609
5	0.96	40±12	232	88	448
10	0.83	30±8	197	86	386
100	0.66	31±8	153	91	308
(b) 1500 Base pair DNA					
0.1	>3	90±46	···	1122	10800
2	0.77	56±28	488	188	1004
5	0.59	52±40	341	145	738
8	0.54	40±20	304	132	662
20	0.50	42±20	259	127	571
200	0.54	30±20	218	117	481
(c) 2311 Base pair DNA					
3	0.37	167±90	726	426	1623
7	0.25	135±14	568	337	1272
27	0.22	135±38	455	258	1014
63	0.24	131±73	419	252	934
103	0.19	266	404	257	901
178	0.21	97±25	394	273	873

Columns:
(2) Ratio of concentration of the DNA used in this study to the overlap concentration calculated with the root-mean-square radius of gyration listed in Table I: $C^*=3/(4\pi R_G^3)$.
(3) Experimental values of DNA first intramolecularl/rotational decay times calculated taking the second peak from CONTIN output as contributed from translational and rotational relaxation, rotational relaxation times were calculated as $\tau_{rot,meas}=1/(\Gamma_2-\Gamma_1)$, where Γ_1 is the decay time of the first peak, and Γ_2 decay time of the second peak from the CONTIN output.
(4) Rotational decay times were calculated using the persistence length listed in column 5 of Table I and the Yoshizaki–Yamakawa formula.
(5) First intramolecular decay times calculated using the root-mean-square radii of gyration listed in Table I and measured diffusion coefficients and the Rouse–Zimm free draining coil model, Eq. (10).
(6) First intramolecular decay times calculated using the root-mean-square radii of gyration listed in Table I and the Rouse–Zimm nondraining coil model, Eq. (12).

are listed in column 3 of Table II. Sorlie and Pecora's results for the 2311 base pair fragment[7,8] at 103 mM Na^+ are also listed in Tables I(c) and II(c) for comparison. The intramolecular decay times from Sorlie and Pecora's experiments on the 2311 and the 1010 bp fragments are larger by about a factor of 2 than the corresponding ones obtained in this work for the 2311 bp fragment at differing salt concentrations and for the 1100 bp fragment at a similar salt concentration. We do not know the reason for this discrepancy. The translational diffusion coefficients as functions of added NaCl are shown in Fig. 5.

The intramolecular decay rates (excluding the point from Sorlie and Pecora) show a clear decreasing trend as the concentration of added salt in solution decreases, while the translational diffusion coefficient first increases and then decreases, going through a maximum. A similar decrease in the intramolecular decay rates was observed previously for the relaxed circular 2311 bp fragment.[5,6] This suggests that as salt concentration in solution decreases, intramolecular electrostatic interactions may result in more rigid, extended conformations of the highly charged DNA molecules. As stated

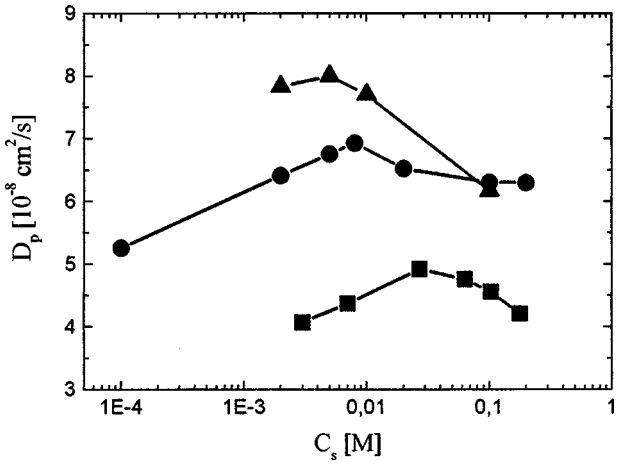

FIG. 5. Translational diffusion coefficients of the three DNAs vs ionic strength: ▲, 1100; ●, 1500; ■, 2311.

in the Introduction, the translational diffusion coefficient is sensitive to both the dimension of the molecule and electrostatic interactions between molecules (including the small ions) in solution. The increasing of the dimensions slows down the translational diffusion; the increasing of intermolecular electrostatic interactions, however, speeds up the translational diffusion. The combined effects lead to the increasing and then decreasing trend of the translational diffusion coefficient as the solution ionic strength decreases. Note (Fig. 5) that the position of the maximum occurs at higher added salt concentrations the higher the molecular weight of the fragment. We discuss some of these effects further in the next sections.

A. Counterion condensation

For all solutions used in this study, *p*H values were kept at 8.0(2311 bp) or 7.6 (1100 and 1500 bp) by buffer exchange and by using fresh solutions. At these *p*H's, the linear DNA fragments are highly negatively charged. For example, there are 4624 phosphate groups on the double helix for the 2311 bp DNA that might be negatively charged. Based on 0.336 nm rise per base pair, the contour length of the DNA is 776 nm. This could result in a DNA charge density up to 8.27 electron charges per nm along the contour length. According to Manning's counterion condensation theory[17,18] the maximum charge density that can be supported in aqueous solution is $1/(N\lambda_B)$, where N is the counterion charge, and the Bjerrum length λ_B at 20 °C is 0.714 nm. The effective charge on this DNA, after counterion condensation, is then estimated to be $Z_{eff}=-1087$. Similarly for the 1500 and 1100 bp fragments, the effective charges are -705 and -517, respectively.

B. Coupled mode model

To estimate the effect of electrostatic interactions on the solution dynamics of the highly charged DNA, the coupled mode theory[1,16,19–21] was used to calculate the translational diffusion coefficients of the fragments for the polyion concentration and salt concentration conditions used in this study. The diffusion coefficients of small ions (Na^+ and

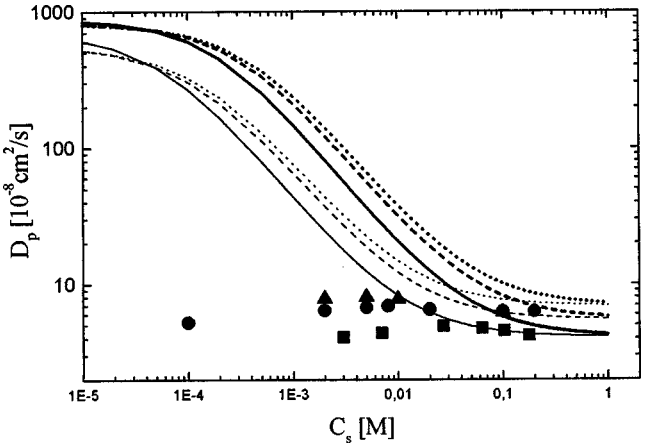

FIG. 6. Dependencies of the calculated (lines) and measured (symbols) translational diffusion coefficients of the 1100, 1500, and 2311 base pair DNA fragments on the added salt concentration. Two sets of calculations are shown: the top set of lines shows the diffusion coefficients obtained from the coupled mode theory using the charges calculated from Manning's counterion condensation theory; the bottom set uses coupled mode theory and half the Manning theory charge. Within each set from top to bottom: 1100, 1500, 2311. Symbols as in Fig. 5.

Cl^-) were taken from experimentally measured self-diffusion coefficients[22,23] converted to those at 20 °C. The anion concentration was calculated from the total added salt concentration; the cation concentration was calculated from both the added salt and DNA concentration. The DNA concentrations in the theoretical calculations were the actual concentrations used in the experiments. The procedure described previously for a 20 bp fragment was used with the appropriate parameters for the longer fragments studied here.[1] The coupled mode theory predictions of the diffusion coefficients of the three DNA fragments for the various experimental conditions are shown in Fig. 6. Calculations were done using both the Manning charge and one-half the Manning charge. In both cases there is, as expected, a large increase in diffusion coefficient predicted at low added salt concentrations. Experimental data for the diffusion coefficients from DLS correlation functions of the DNA fragments measured at 20 °C from Fig. 5 are also plotted in Fig. 6 for comparison with the theoretical results.

In our studies of the 20 bp duplex oligonucleotide,[1,2] coupled mode theory together with counterion condensation theory was found to give good agreement with experiments for this highly charged rodlike (but relatively small) polyelectrolyte. (We should, however, note that a diffusion virial theory also gave good agreement with experiment at the lowest concentrations.) Calculations using diffusion coefficients measured at high added salt concentrations as the diffusion coefficients of the 20 bp oligonucleotide with no electrostatic interactions gave very good predictions for the translational diffusion coefficients at all salt concentration and polyion concentrations studied. However, as shown in Fig. 6, using the measured high salt diffusion coefficient of the DNA fragments and the Manning charge results in rather large calculated diffusion coefficients for all salt concentrations. The discrepancy between measured and calculated diffusion coefficients becomes larger at the low added salt concentrations.

The coupled mode model is not likely to give accurate predictions for a highly charged, long, semiflexible polyion since the point charge approximation of the Poisson–Boltzmann equation, on which the coupled mode theory is based, is not applicable. The electrostatic potential around a DNA of total charge of -1087 (for the 2311 bp DNA) is not the same as the electrostatic potential calculated for a point of such high charge. Small ions could, in fact, penetrate the ''interior'' of the polyion and perhaps drag segments of the macroion around instead of speeding up the translational diffusion of the whole macroion. Another source of discrepancy could be from the effective charge calculated from Manning's counterion condensation theory, which, strictly speaking, is only applicable to rodlike polyelectrolytes. The flexibility of the DNA fragments may result in a shorter distance between non-nearest-neighbor segments, causing a higher degree of counterion condensation. Such effects have been shown in recent computer simulations.[24–26] Thus, the combination of coupled mode and counterion condensation theory is not expected to give quantitative results for these DNAs. Our calculations, however, do indicate that, if the polyions maintained their size, their diffusion coefficients would increase as the added salt concentration is lowered. An increase in the polyion size would, of course, tend to decrease the diffusion coefficient.

C. Persistence length and excluded-volume effect

Several groups have developed relations between structural parameters of neutral macromolecules and the translational and rotational diffusion coefficients. Using the Oseen–Burgers procedure, Yamakawa and Fujii[27] derived equations for the translational diffusion coefficient of a wormlike chain in terms of the reduced length $L'=L/2P$ and reduced diameter $d'=d/2$, where P is the persistence length and L is the contour length. The Yamakawa–Fujii equations apply to macromolecules of both long and short lengths. Yoshizaki and Yamakawa[28] derived equations relating the rotational decay time of a helical wormlike chain to the persistence length P via the contour length L and rotational decay time of a rigid rod with length L. Their result is estimated to be valid for reduced lengths $L'<30$. For shorter wormlike chains, Hagerman and Zimm[29] derived a relation between the rotational relaxation times of the wormlike coil and the persistence and contour lengths using a Monte Carlo analysis. In the length scale range studied ($0.1<L/P<5$), the excluded volume effect can be neglected.

Thus, using these theories, persistence lengths can be calculated from the translational or rotational diffusion coefficients. The diffusion coefficients can be probed with dynamic light scattering. However, as shown earlier, electrostatic interactions likely contribute significantly to the translational diffusion coefficients of polyions and there is as yet no practical theory that quantitatively predicts the effect of electrostatic interactions on the diffusion coefficients of long semi-flexible highly charged polyelectrolytes. The rotational diffusion coefficients are, for semiflexible polymers, difficult to measure accurately using dynamic light scattering

due to their small amplitude and mixing with intramolecular decay modes. Persistence lengths obtained by different investigators are often not consistent. There is as yet no consensus on the effects of ionic strength on polyelectrolyte persistence length.[30–39] We give an analysis of the effects of electrostatic interactions on the persistence length of our DNAs based on our dynamic measurements, the Yamakawa–Fujii relation,[27] and the Odijk–Houwaart theory.[36]

Odijk and Houwaart[36] treated the electrostatic contribution to the solution dynamics of flexible polyelectrolytes as two parts: a short range interaction giving rise to an electrostatic persistence length that depends on the Debye–Huckel radius, and a long range interaction denoting the electrostatic excluded volume effect. Their equation for the mean-square radius of gyration reflects both the short range and long range electrostatic interactions,

$$\langle R_G^2\rangle = \tfrac{1}{3}L(P+P_{\mathrm{el}})\{0.541 + 0.459[1+4.43L^{1/2}\kappa^{-1}(P+P_{\mathrm{el}})^{-(3/2)}]^{0.46}\}, \tag{5}$$

where L is the contour length, and κ is the reciprocal Debye length. The electrostatic contributions to the persistence length, P_{el}, at any solution ionic strength condition can be calculated with Eq. (6),

$$P_{\mathrm{el}} = \tfrac{1}{12}\lambda_B Z_{\mathrm{eff}}^2 h(\kappa L), \tag{6}$$

where

$$h(y) = \exp(-y)\left(\frac{1}{y}+\frac{5}{y^2}+\frac{8}{y^3}\right)+\frac{3}{y^2}-\frac{8}{y^3}. \tag{7}$$

Results for calculated electrostatic persistence lengths for the linear DNA fragments at different added salt concentration conditions are listed in Table I. To calculate the total persistence length, the intrinsic (bare) persistence length, P, of the DNA (without electrostatic effects) is needed.

We assume that the electrostatic contribution to the persistence length and the mean-square radius of gyration is small at high salt concentration conditions. Taking the translational diffusion coefficient measured for the 2311 bp DNA at 178 mM salt conditions, and using the Yamakawa–Fujii theory,[27] we obtain an apparent persistence length of 53.5 nm.

The mean-square radius of gyration for a wormlike chain can be calculated from the contour length L and the apparent persistence length P_{app} using the Benoit–Doty equation,[40,41]

$$\langle R_G^2\rangle = P_{\mathrm{app}}^2\{L/(3P_{\mathrm{app}})-1+2P_{\mathrm{app}}/L - 2[1-\exp(-L/P_{\mathrm{app}})]/(L/P_{\mathrm{app}})^2\}. \tag{8}$$

Applying $P_{\mathrm{app}}=53.5$ nm, $\langle R_G^2\rangle$ of the 2311 bp DNA at 178 mM added salt concentration conditions is calculated to be 106.5 nm. The bare persistence length of the DNA can now be calculated from this radius of gyration and Eq. (5). P_{el} may then be calculated at different ionic strengths from Eq. (6). Thus, the total persistence length, $P_T=P_{\mathrm{el}}+P$, and $\langle R_G^2\rangle$ can be calculated for the DNA at each ionic strength. Results for all the DNA fragments are listed in Table I. The root-mean-square radius of gyration listed in column 5 of Table I can be verified, in principle, using static light scattering, but the amounts of materials available to us were too small to perform these direct measurements. An apparent persistence length (also shown in Table I was calculated for all salt concentrations using the Odijk–Houwaart $\langle R_G^2\rangle$ and the Benoit–Doty relation.

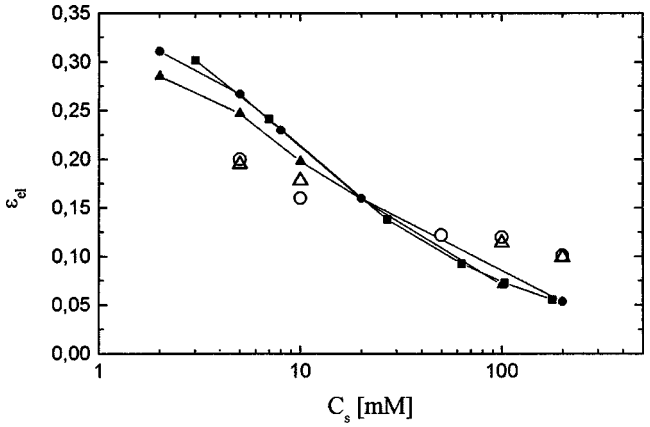

FIG. 7. Excluded-volume parameters of the DNAs vs added salt concentration. Values are calculated using Eq. (9): ▲, 1100; ●, 1500; ■, 2311. Also shown are parameters reported by Ross and Scruggs (Ref. 35) for high molecular weight bacteriophage DNA obtained from viscosity measurements (△) and for Col E_1 DNA calculated by Borochov, Eisenberg, and Kam (Refs. 32, 33) using root-mean-square radii of gyration and excluded-volume corrected persistence lengths (○).

The electrostatic excluded-volume parameter ϵ_{el} can be calculated from

$$\epsilon_{\mathrm{el}} = \left(\frac{3^{3/2}}{4\pi^{1/2}}\right)L^{1/2}\kappa^{-1}P_T^{3/2}. \tag{9}$$

Results for the electrostatic excluded-volume parameter are listed in Table I. In addition, the ϵ_{el} for the fragments studied are shown along with results of other workers on high molecular weight DNAs in Fig. 7. Ross and Scruggs studied polyelectrolyte expansion effects on high molecular weight DNA by viscosimetry.[38] Their intrinsic viscosity measurements indicate that DNA never shows the characteristic scaling parameter for random coil polyelectrolytes, even in the limit of infinite ionic strength. Their excluded-volume parameters for the DNA were calculated with the Flory hydrodynamic theory. Borochov, Eisenberg, and Kam,[32,33] calculated the excluded-volume parameter for Col E1 DNA from its root-mean-square radius of gyration measured by total intensity light scattering and the Sharp and Bloomfield theory.[39] As shown in Fig. 7, the results are in good agreement with each other. All show a decrease of the excluded-volume parameter as the added salt concentration increases.

The apparent persistence lengths listed in Table I can be compared with results from total intensity light scattering and Eq. (8) without correction for excluded volume and electrostatic interactions. As shown in Fig. 8, the apparent persistence lengths agree with the persistence lengths calculated for Col E_1 DNA by Borochov, Eisenberg, and Kam[32] using the Benoit–Doty equation and the root-mean-square radii of gyration measured without applying an intramolecular

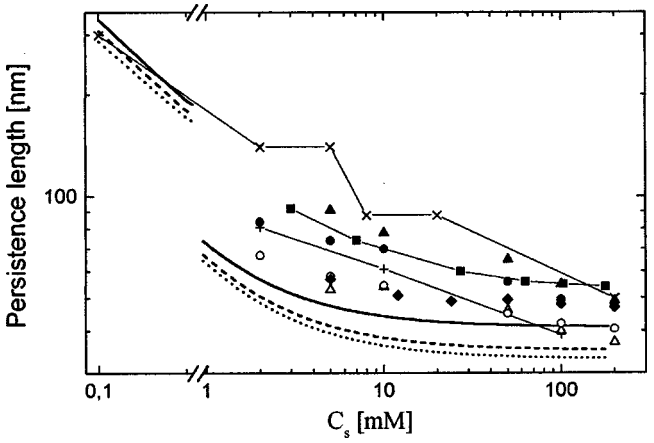

FIG. 8. Ionic strength dependencies of persistence lengths of DNA. Apparent persistence lengths of the DNAs calculated using the Benoit–Doty relation for a wormlike chain and root-mean-square radii of gyration from Table I (■, 2311; ×, 1500; +, 1100). The total persistence length as a sum of bare persistence length and electrostatic persistence length: solid line 2311, dashed line 1500, dotted line 1100. Also shown are the persistence lengths calculated for Col E_1 DNA by Borochov, Eisenberg, and Kam (Refs. 32, 33) using the Benoit–Doty relation and root-mean-square radii of gyration measured with static light scattering, assuming the intramolecular excluded-volume can be neglected (▲), and with an excluded-volume correction (△). Persistence lengths reported by Cairney and Harrington (Ref. 34) for *T*7 phage DNA taking the DNA optical anisotropy=−12.389 (●), and optical anisotropy=−12.978 (○), and those reported by Rizzo and Schellman (Ref. 35) for *T*7 DNA (♦) are also given.

excluded-volume correction. Also in close agreement are persistence lengths calculated by Cairney and Harrington[34] for T7 phage DNA from flow birefringence data taking the optical anisotropy for DNA as −12.389 and without an excluded-volume correction. Rizzo and Schellman[35] calculated persistence lengths of T7 DNA from flow dichroism data and the Zimm theory for flexible coils and their values lie below our calculated apparent persistence lengths.

The sum of intrinsic (bare) and electrostatic persistence lengths are close to those corrected for excluded-volume effects by Borochov, Eisenberg, and Kam[32,33] for Col E_1 DNA. Our results show that the persistence length reaches a plateau at a lower added salt concentration than that of Borochov *et al*. The discrepancy may arise from possible contributions of the electrostatic interactions at the highest added salt concentrations, which we assumed had negligible effects on the translational diffusion coefficient.

D. Diffusion and intramolecular relaxation

The translational diffusion coefficients for the DNAs at each concentration of added salt were calculated using the apparent persistence lengths given in Table I and the Yamakawa–Fujii theory.[27] The results are listed in Table I for comparison with experimentally observed translational diffusion coefficients. The calculated translational diffusion coefficients decrease as the added salt concentration decreases due to an increased persistence length. Clearly, this alone can not explain the maximum of the diffusion coefficient. Even though the coupled mode theory is not successful in predicting translational diffusion coefficients for this DNA, the coupling between the diffusion of small ions with that of the DNA is still likely to be a major factor increasing the DNA diffusion coefficient as the concentration of added salt decreases. As the added salt concentration decreases, electrostatic interactions produce two effects on the translational diffusion coefficients of the DNA: intramolecular electrostatic interactions enhance the stiffness of the molecule, resulting in an increasing persistence length and, thus, a decreasing translational diffusion coefficient. On the other hand, intermolecular electrostatic interactions result in an increased coupling between small ion diffusion and polyion diffusion, thus driving the DNA to diffuse faster. The combination of these two opposing effects results in the observed increasing and then decreasing trend of the DNA diffusion coefficient as the added salt concentration decreases.

DLS studies of the circular 2311 base pair DNA by Seils and Pecora[5] and Newman, Tracy, and Pecora[6] also indicated a steady increase in the persistence length and in the radius of gyration as the added salt concentration decreases. Both, however, showed a relatively constant measured translational diffusion coefficient in the salt concentration ranges studied. By not considering the effect of small ions on the diffusion of polyions, however, they could not explain their observed salt concentration dependence of the translational diffusion coefficient of the DNA.

To determine if the second relaxation time observed by dynamic light scattering is from end-to-end rotational relaxation of the DNA, the theoretical treatment of Yoshizaki and Yamakawa[28] for helical wormlike chains was applied using the apparent persistence lengths shown in Table I. The calculated rotational relaxation times listed in Table II show a very strong ionic strength dependence and are too large compared to experimentally observed relaxation times. This indicates that the observed second mode by dynamic light scattering for these fragments is probably not from a pure rotational relaxation process. Thus, for these systems, it is not appropriate to calculate persistence lengths from the experimentally observed second mode relaxation times (or vice versa) using the Yoshizaki–Yamakawa theory. It should be pointed out that the concept of ''rotational relaxation'' for a flexible chain or coil is ambiguous, as the molecule is constantly changing its conformation due to internal relaxation.

The Rouse–Zimm coil models[41–44] can be used to calculate the first intramolecular relaxation time from the DNA translational diffusion coefficient and radius of gyration at each of the salt concentrations studied. By using the theoretical radii of gyration and the experimental translational diffusion coefficients in the calculation, some stiffness of the chain is incorporated in the model.

The intramolecular decay time of normal modes predicted by the Rouse–Zimm free-draining model[41,42] can be calculated from the radius of gyration and the translational diffusion coefficient

$$\tau_k = \frac{\langle R_G^2 \rangle}{\pi^2 D k^2}, \quad k = 1,2,...,N. \tag{10}$$

Seils and Pecora[5] have presented arguments that this basic

scaling of τ_k with the mean-square radius of gyration and diffusion coefficient is valid even for semiflexible macromolecules.

Zimm[42] considered hydrodynamic interactions in modeling the dynamics of a flexible chain in solution. He used the Kirkwood–Riseman method[43] to incorporate hydrodynamic interactions through the Oseen interaction tensor in the Rouse flexible Gaussian coil model.[44] The resulting diffusion coefficient for the ''nondraining'' case can be written in the form

$$D = 0.192 k_B T/(\eta_0 R_G), \tag{11}$$

where η_0 is the solvent viscosity and R_G is the root-mean-square radius of gyration. The internal decay times in the nondraining model are

$$\tau_k = 11.8 \eta_0 R_G^3/k_B T \lambda_k, \quad k = 1,2,...,N. \tag{12}$$

The λ_k are constants that have been calculated for the longest wavelength modes ($\lambda_1 = 4.04$).[41]

The Rouse–Zimm free-draining model and nondraining model relaxation times are listed in Table II for comparison with experimental data. Neither model gives a good representation of the measured times, although the free draining model is closer than the nondraining model. Seils and Pecora reached a similar conclusion for the relaxed circular 2311 bp fragment.[5]

We have also explicitly examined the Seils–Pecora scaling law by calculating the root-mean-square radius of gyration from the relation

$$\langle R_G^2 \rangle \propto \tau_1 D, \tag{13}$$

where the proportionality constant in Eq. (13) is assumed to be insensitive to the added salt concentration. The results, calculated using the high salt radius of gyration as a reference, are shown in column 10 of Table I. The trends generally follow those in column 6, but there are discrepancies. This is not surprising given the uncertainties in both τ_1 and the numbers in column 6.

IV. CONCLUSION

We have used dynamic light scattering-photon correlation spectroscopy to measure the added salt concentration and scattering angle dependencies of the translational diffusion coefficient and the first intramolecular relaxation time of three linear, monodisperse DNA fragments. The translational diffusion coefficients of the fragments were obtained from light scattering intensity autocorrelation functions measured at the lowest scattering angle where only one peak appears in the DLS frequency distribution. As the scattering angle increases, the contribution of internal relaxation processes to the autocorrelation function become more important and the first peak in the decay rate distribution becomes wider and shifts to higher decay rates. A second mode that appears at intermediate scattering angles was interpreted as arising from combined translation/intramolecular relaxation, following previous work on DNA fragments. As the added salt concentration was decreased, the first intramolecular mode showed a decreasing rate, and the translational diffusion coefficient, although relatively constant, showed a maximum for all three fragments. An alternative analysis to the coupled mode approach that predicts a large increase in the diffusion coefficient as the added salt concentration is lowered was used to characterize the dynamics of these relatively long and flexible fragments. The contribution of electrostatic interactions was treated as a combination of short-range and long-range interactions following the Odijk–Houwaart procedure. Assuming that for the highest added salt concentration conditions, the effects of electrostatic interactions on the translational diffusion coefficients can be ignored, a bare persistence length of the DNA was obtained using the Yamakawa–Fujii equation. The total persistence length was then calculated as the sum of this bare (intrinsic) persistence length and the theoretical electrostatic persistence length determined by Odijk and Houwaart. The radii of gyration of the DNAs, including the excluded-volume effect, were then calculated at each solution ionic strength. Apparent persistence lengths were calculated from these theoretical radii of gyration and the Benoit and Doty equation. The calculated persistence lengths of DNA at various added salt concentration conditions are consistent with results obtained by other researchers. The apparent persistence length is the quantity that can be compared with and used with theoretical formulas derived for the dynamics of uncharged polymers.

The relaxation times for the intramolecular modes are generally smaller than those predicted by the free-draining Rouse–Zimm model for the coil slowest intramolecular relaxation mode. There is some support that the scaling suggested by previous workers[5] between the first intramolecular mode relaxation time and the ratio of the mean-squared radius of gyration and the diffusion coefficient is a general result for semiflexible chains.

As the added salt concentration decreases, the translational diffusion coefficient decreases due to the increasing persistence length of the chain. The coupling between small ion diffusion and polyion diffusion is thought to partially counteract this effect and to tend to increase the DNA diffusion coefficient. The combination of these two opposing effects results in the appearance of a maximum in the measured translational diffusion coefficient of the DNA as the added salt concentration decreases.

ACKNOWLEDGMENTS

This work was supported by the National Science Foundation (USA) Grant No. CHE-9520845 to R.P., the U.S.–Polish Marie Sklowdowska-Curie Joint Fund II Grant No. MEN/NSF-96-254, the Volkswagen Stiftung, Federal Republic of Germany and NATO Cooperative Linkage Grant No. 975728. We are grateful to Dr. Damian Labuda of the University of Montreal for providing us with the 1100 and 1500 bp DNA PCR fragments.

[1] H. Liu, L. Skibinska, J. Gapinski, A. Patkowski, E. W. Fischer, and R. Pecora, J. Chem. Phys. **109**, 7556 (1998).
[2] L. Skibinska, J. Gapinski, H. Liu, A. Patkowski, E. W. Fischer, and R. Pecora, J. Chem. Phys. **110**, 1794 (1999).
[3] R. J. Lewis, J. H. Huang, and R. Pecora, Macromolecules **18**, 1530 (1985).
[4] J. Seils and R. Pecora, Macromolecules **28**, 661 (1995).
[5] J. Seils and R. Pecora, Macromolecules **25**, 354 (1992).
[6] J. Newman, J. Tracy, and R. Pecora, Macromolecules **27**, 6808 (1984).

[7] S. S. Sorlie and R. Pecora, Macromolecules **21**, 1437 (1988).
[8] S. S. Sorlie and R. Pecora, Macromolecules **23**, 487 (1990).
[9] R. J. Lewis and R. Pecora, Macromolecules **19**, 2074 (1986).
[10] R. J. Lewis, J. H. Huang, and R. Pecora, Macromolecules **18**, 944 (1985).
[11] S. W. Provencher, Makromol. Chem. **180**, 201 (1979).
[12] S. W. Provencher, Comput. Phys. Commun. **27**, 213 (1982); **27**, 229 (1982).
[13] S. W. Provencher, J. Hendrix, L. De Maeyer, and N. Paulussen, J. Chem. Phys. **69**, 4273 (1978).
[14] R. Pecora, J. Chem. Phys. **43**, 1562 (1965).
[15] R. Pecora, J. Chem. Phys. **49**, 1032 (1968).
[16] B. J. Berne and R. Pecora, *Dynamic Light Scattering* (Wiley, New York, 1976).
[17] G. S. Manning, J. Chem. Phys. **51**, 924 (1969); **51**, 934 (1969); **51**, 3249 (1969).
[18] G. S. Manning, Q. Rev. Biophys. **11**, 179 (1978).
[19] S. C. Lin, W. I. Lee, and J. M. Schurr, Biopolymers **17**, 1041 (1978).
[20] P. Tivant, M. Turq, M. Drifford, R. Magdelenat, and R. Menez, Biopolymers **22**, 643 (1983).
[21] K. Schmitz, Macromolecules **27**, 3442 (1994).
[22] J. H. Wang and S. Miller, J. Am. Chem. Soc. **74**, 1611 (1952).
[23] J. H. Wang, J. Am. Chem. Soc. **74**, 1612 (1952).
[24] R. G. Winkler, M. Gold, and P. Reineker, Phys. Rev. Lett. **80**, 3731 (1998).
[25] M. J. Stevens and K. Kremer, J. Chem. Phys. **103**, 1669 (1995).
[26] J. C. Chu and C. H. Mak, J. Chem. Phys. **110**, 2669 (1999).
[27] H. Yamakawa and M. Fujii, Macromolecules **6**, 407 (1973).
[28] T. Yoshizaki and H. Yamakawa, J. Chem. Phys. **81**, 982 (1984).
[29] P. J. Hagerman and B. H. Zimm, Biopolymers **20**, 1481 (1981).
[30] R. J. Lewis, D. Eden, and R. Pecora, Macromolecules **19**, 134 (1986).
[31] R. E. Harrington, Biopolymers **17**, 919 (1978).
[32] N. Borochov, H. Eisenberg, and Z. Kam, Biopolymers **20**, 231 (1981).
[33] Z. Kam, N. Borochov, and H. Eisenberg, Biopolymers **20**, 2671 (1981).
[34] K. L. Cairney and R. E. Harrington, Biopolymers **21**, 923 (1982).
[35] V. Rizzo and J. Schellman, Biopolymers **20**, 2143 (1981).
[36] T. Odijk and A. C. Houwaart, J. Polym. Sci. Polymer. Phys. E **16**, 627 (1978).
[37] J. Skolnick and M. Fixman, Macromolecules **10**, 944 (1977).
[38] P. D. Ross and R. L. Scruggs, Biopolymers **6**, 1019 (1968).
[39] P. Sharp and V. A. Bloomfield, Biopolymers **6**, 1201 (1968).
[40] H. Benoit and P. Doty, J. Phys. Chem. **57**, 958 (1953).
[41] H. Yamakawa, *Modern Theory of Polymer Solutions* (Harper and Row, New York, 1971).
[42] B. H. Zimm, J. Chem. Phys. **24**, 269 (1956).
[43] J. G. Kirkwood and J. Riseman, J. Chem. Phys. **16**, 565 (1948).
[44] P. E Rouse, J. Chem. Phys. **21**, 1272 (1953).